Physics of Viral Shells

ROBIJN F. BRUINSMA

Department of Physics and Astronomy, University of California, Los Angeles,

Department of Chemistry and Biochemistry, University of California, Los Angeles

WILLIAM S. KLUG

Department of Mechanical and Aerospace Engineering, University of California, Los Angeles

Key Words viral capsid, statistical mechanics, elasticity theory, structural phase transition, Landau theory

Abstract We review the application of statistical mechanics, elasticity theory, and condensed-matter physics to the assembly and maturation of viral capsids.

CONTENTS

List of Figures

1 Introduction

In 1955 Fraenkel-Conrat and Williams [1] showed that the rod-like Tobacco Mosaic Viruses (TMV) assembles spontaneously in solutions containing the molecular components of the virus (capsid proteins and the RNA genomic molecules). Because of their highly reproducible size and shape and their precise structural organization, the shells of viruses, or *capsids* have since found many applications in materials science. Directed evolution of the capsid proteins allows attachment of particular receptor groups on the exterior surface. Functionalized viral shells have been used to create metallic wires, solar cells, batteries, and fuel cells [2]. This review discusses the application of methods borrowed from statistical physics, condensed matter physics, soft-matter physics and elasticity theory to the self-assembly and material properties of viral capsids.

2 The Structure of Viral Capids

2.1 The Cowpea Chlorotic Mottle Virus

Figure 1 shows the *Cowpea Chlorotic Mottle Virus*, a roughly spherical virus with a radius of about 15 nm that infects the cowpea plant. Like TMV, CCMV self-assembles spontaneously [3]. The physical properties of CCMV have been extensively studied and it also is applied extensively in material and medical science. Panel A of the figure shows an image of the CCMV capsid, reconstructed by Cryo Transmission Electron Microscopy and X-ray Diffraction methods [4, 5]. The regular surface structure of the CCMV capsid resembles a crystal and, like a crystal, it can be characterized by its *symmetry operations*. Figure 1A is oriented along a two-fold symmetry axis. The capsid also has three-fold and five-fold rotation axes. The various rotational symmetry operations coincide with those of the *icosahedron* (see Fig. 1B). Note that the image of Figure 1A

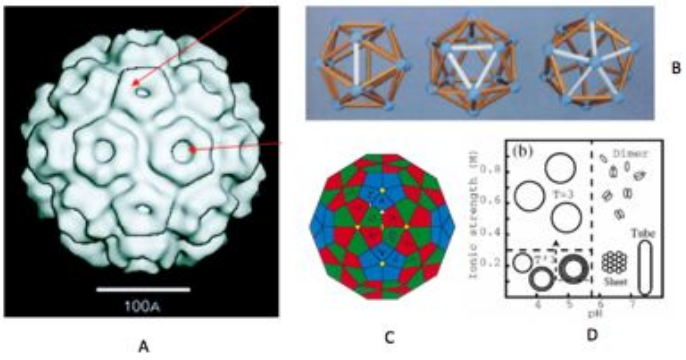

Figure 1: Structure and assembly of CCMV. A) Cryo Transmission Electron micrograph [5]. The red arrows indicate pentamers and hexamers. B) The two-fold, three-fold, and five-fold symmetry axes of an icosahedron. C) Locations of the capsid proteins in the CCMV shell. Symmetry-equivalent proteins have the same color (from the lab of J. Johnson). D) Assembly diagram of CCMV capsids [6]. The horizontal axis is the pH level. The vertical axis is the salinity.

has the orientation of the first panel of Fig. 1B.

The red arrows in Fig. 1A indicate ring-like structures with apparent six-fold and five-fold symmetry known as "hexamers", respectively, "pentamers". They are composed of six, respectively, five capsid proteins (CPs). CCMV capsids have in total twelve identical pentamers and twenty identical hexamers so in total 180 identical CPs. Figure 1C shows schematically how the 180 proteins are distributed over the shell. Proteins in symmetry-equivalent positions are indicated by the same color. Sixty pentamer proteins are marked red. Sixty hexamer proteins are marked green (B) and another sixty blue (C).

Finally Fig. 1D shows the assembly diagram of CCMV capsids in a solution of CPs [6]. The vertical axis is the ionic strength I, the salt concentration and the horizontal axis is the pH ($I \sim 0.1$ and $pH \sim 7$ under typical physiological conditions). In an aqueous physiological solution, CCMV CPs form dimers at low protein concentrations

(typically in the microMolar range). Hexagonal layers or spherocylinders form at higher concentrations. Reducing the pH to below the physiological level leads to the formation of CCMV capsids at higher I values and concentric multi-shells at lower I. The fact that reducing the salinity stimulates aggregation is an indicator that electrostatics plays an important role in the interactions between CPs. In the Debye-Hückel (DH) theory of aqueous electrostatics, the range of electrostatic interactions is inversely proportional to $I^{1/2}$ [7]. The reason for the dependence of CCMV capsids on the acidity level is discussed below. If viral RNA molecules are included in the solution, then infectious viruses will assemble at reduced pH. In this review, we will focus exclusively on empty capsids.

2.2 The Amphiphilic Capsid Protein.

Figure 2 shows schematically the structure of a typical CP as obtained from X-ray diffraction studies of crystals composed of viruses,[5] (maximum resolution currently in the range of an Angstrom). CPs are, like all proteins, composed of chains of amino acids, or "residues", linked by chemical bonds, together forming the "primary structure" of the protein. The polymeric backbone is indicated in Fig. 2 as a light gray tube that winds around inside the prismatic outline [8]. The end points of the primary structure of a protein are known as the N and C terminals and are indicated in Fig. 2. Parts of the chain that are highlighted as parallel colored arrows are sections of the main chain whose residues are linked by hydrogen bonds. These "β sheets" provide rigidity to the spatial structure of the CP. The CPs of a large number of viruses share this particular structural motif, which is known as the "jelly roll" [8], even when they may have very different primary amino acid sequences.

The top and bottom surfaces of the CP outline are lined with *hydrophilic* residues,

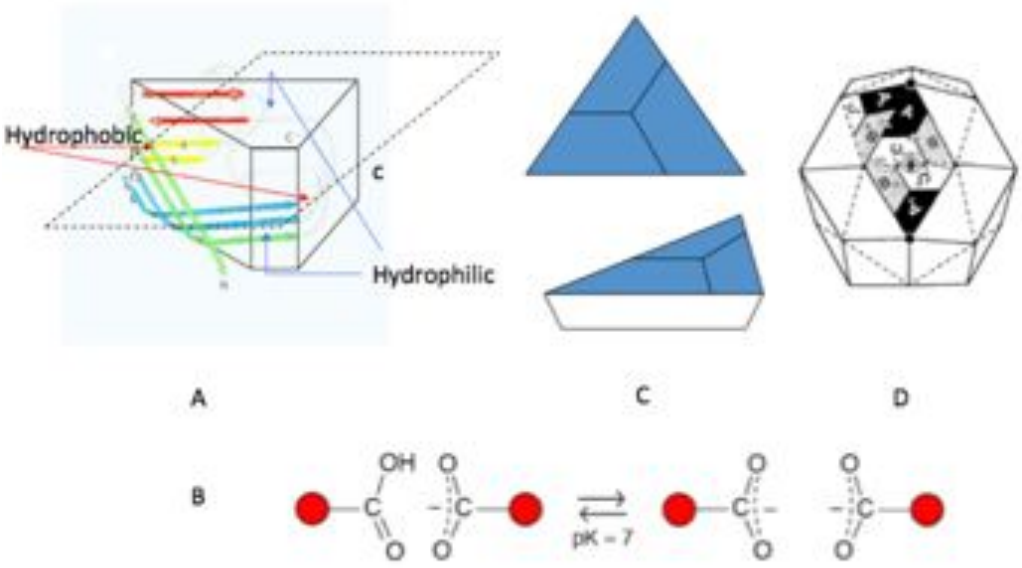

Figure 2: Capsid Proteins. A) The jelly roll folding motif (from [8]). The amino acid backbone is shown as a grey tube while β sheets are indicated by parallel arrows. The outlined vertical surfaces are hydrophobic while the horizontal surfaces are hydrophilic. The outlined midplane shows that CPs do not have an up-down mirror plane. B) Attractive pairing between residues of different capsid proteins (from [9]). C) Three proteins fit together to form an equilateral triangle with slanted edges. D). Sixty triangles fit together to form small virus.

some charged, while *hydrophobic* residues line the vertical sides of the protein. Molecules that have both hydrophobic and hydrophilic exposed groups are known as *amphiphiles*. The phase diagram of amphiphiles has been extensively studied in the context of soft-matter physics [7] with surfactants and lipids as the favorite examples. Surfactant and lipids in dilute aqueous solution tend to assemble spontaneously and reversibly into aggregates that may be spherical (micelles and vesicles), planar (e.g. the L_α phase), or

three-dimensional (e.g. the L_3 phase). These aggregates often constitute minimum free energy states but they typically are delicate and subject to strong thermal fluctuations [7]. The spontaneous formation of capsids from CPs in aqueous solution has some similarity with amphiphilic self-assembly, but there are also important differences as we shall see.

The hydrophobic edges of the CPs can be matched together so water molecules are expelled from the shared interface. In addition, specific residues are capable of pair formation across the shared interface [9]. CPs have very large electrical dipole moments with (for CCMV) about ten negative charges on the surface facing the exterior of the virus and a similar number of positive charges facing the interior. The *net* electrostatic charge is however modest and changes sign as a function of the pH level because of protonation/deprotonation of certain CP residues. Capsid assembly is possible only if the electrostatic repulsion between two adjacent CP dipoles — which is in the range of ten's of k_BT — is overcome by hydrophobic attraction [10] [1]. The reason that CCMV capsids do not form under physiological conditions is that in that regime the electrostatic repulsion is strong enough to overcome the attractive interactions. Reducing the pH reduces the electrostatic charge of certain CP residues sufficiently to allow for capsid assembly. Reducing pH also enhances the pairing interactions.

We will need a coarse-grained representation in the form of simple building blocks. One possible choice is shown in Figure 2B, where a CP is outlined as a prism with a parallelogram base that has two interior angles of 60 degrees and two interior angles of 120 degree. The vertical surfaces are hydrophobic; the horizontal surfaces hydrophobic. Three of these prisms can be assembled into a triangular truncated pyramid, as shown in

[1] The electrical fields surrounding CPs are so strong that DH theory cannot be applied to viral assembly. Interesting effects of aqueous electrostatics in the strong charging regime, such as counterion condensation and release, correlation attraction, and overcharging may well play an important role in viral assembly but this is not yet well understood.

Figure 2C. By changing the slant of the edges of the blocks, one can fabricate a range of "deltahedral shells" shells with different radius. The assembly of deltahedral shells is also a convenient model for studying viral assembly by numerical simulation [11, 12, 13]. The smallest shell of this type is the icosahedron, composed of twenty triangular blocks, so 60 proteins in total (known as a T=1 shell). The next smallest shell, shown in Figure 2D, is composed of 60 blocks, so the same number of proteins as for CCMV. Though this shell does not look much like CCMV, it is in fact a reasonable representation of the capsid of certain other viruses (such as the noda and picornaviruses). [2]

2.3 The Caspar-Klug Construction

One can construct a systematic "crystallography" for deltahedral shells with icosahedral symmetry of any size [15]. Start from a flat hexagonal sheet composed of triangles and draw the lattice vector $\vec{A}(h,k) = h\hat{a}_1 + k\hat{a}_s$ in the hexagonal sheet. Here, $\{h,k\}$ is a pair of integers and $\hat{a}_{1,2}$ are a pair of basis vectors of the hexagonal lattice (see Fig. 3). Next, complete an equilateral triangle that has $\vec{A}(h,k)$ as its base. The vertices of the triangle are lattice sites of the hexagonal sheet. Cut out twenty identical equilateral triangles from the hexagonal layer and assemble then together in the form of icosahedron. This construction can be carried out for every pair of integers h and k. Figure 3 shows examples with $h = 1, k = 1$ and $h = 2, k = 1$. In general, the size of the icosahedron is determined by the length of the base vector $\vec{A}(h,k)$. It follows from trigonometry that $|\vec{A}(h,k)|^2$ equals $T(h,k) = h^2 + k^2 + hk$. The *triangulation number*, T, specifies the number of inequivalent CP positions in the lattice. For instance a $T = 1$ capsid has one class of lattice positions, with all CPs equivalent by icosahedral symmetry. The $T = 3$ shell has

[2] This "building block" description probably leaves out important physics. CPs in solution in solution are likely to have a different configuration from CPs that are part of a capsid. In addition, CPs that are part of capsids may exhibit strong structural fluctuations [14].

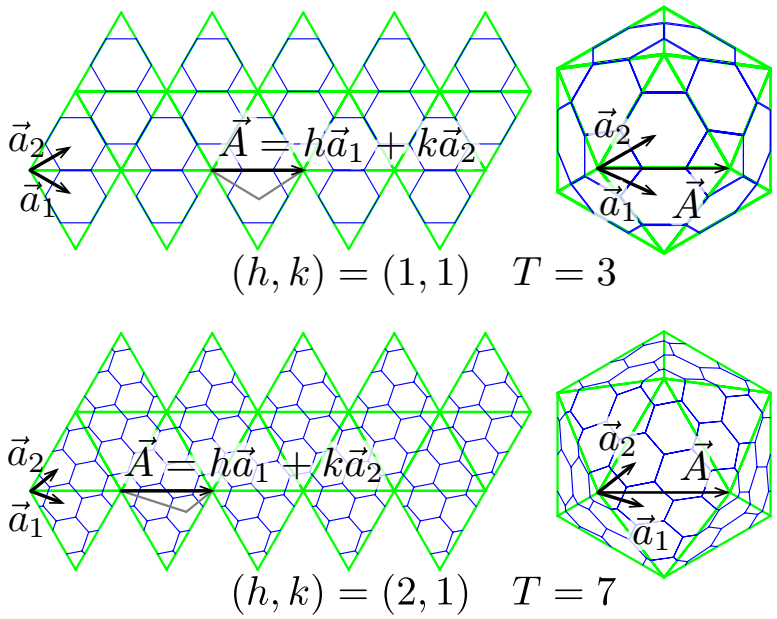

Figure 3: Caspar-Klug Construction: $T = 3$ and $T = 7$(laevo) shells are constructed from hexamer lattices by gluing the edges of the folding template. Notice that $T = 7$ is a chiral structure, $(2,1) \not\equiv (1,2)$, while $T = 3$ is achiral.

three inequivalent positions (fig. 1); each icosahedral face is three-fold symmetric, with each of the three crystallographic units containing one protein from a pentamer (blue in fig. 1), and two proteins from a hexamer (red and green in fig. 1). Likewise for $T = 7$ (fig. 3) each crystallographic unit covers a CP from one pentamer and all six proteins from one hexamer. The total number of proteins is then T CPs per unit times 3 units per face times 20 faces, or $N = 60T$, organized into 12 pentamers and $10(T-1)$ hexamers.

This is the Caspar-Klug (CK) construction that remains the basis of structural virology. Every virus with an icosahedral shell has a characteristic T-Number. As an example, Fig. 4 shows a micrograph of the Hong Kong 97 virus, or HK97, a bacteriophage virus with a double stranded DNA genome [16]. HK97 is quite a bit larger than CCMV. It has an icoosahedral shell composed of twelve pentamers and sixty hexamers consistent with a $T = 7$ shell with $h = 2$ and $k = 1$. Interestingly, $T = 7$ shells are *chiral*. Construct a

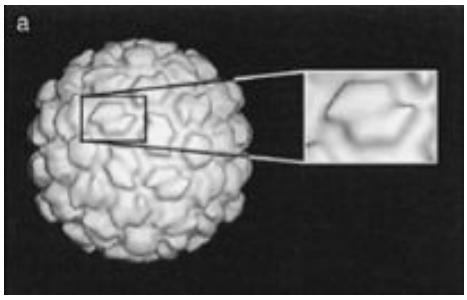

Figure 4: Cryo-electron micrographs of the HK97 viral capsid. Note that the hexamers are strongly sheared.

$T = 7$ shell from the vector $\vec{A}(h = 2, k = 1)$ by taking two steps along the $\hat{a}_1$ axis of the hexagonal lattice and then one step along $\hat{a}_2$. An alternative manner to construct a $T = 7$ shell is to start from the *mirror reflection* of $\vec{A}(h,k)$ along the $\hat{a}_1$ axis, which corresponds to $h = 1$ and $k = 2$. The resulting shell is the mirror image. Using the conventions of chemistry, they are denoted as *laevo* and *dextro*. Because CPs are composed of chiral amino acids, dextro and laevo shells must have different energies so $T = 7$ shells should have a definite handedness. HK97, for example, is *laevo*. The chirality of HK97 will play an important role later on.

3 The Statistical Mechanics of Capsid Assembly

The equilibrium self-assembly by "classical" amphiphilic molecules (like lipids and surfactants) is well understood through the application of basic statistical mechanics methods [7] and in this section we apply these same methods to the self-assembly of capsids by CPs [17].

3.1 The Cluster Size-Distribution Function

The self-assembly of capsids normally takes place under conditions of fixed temperature and pressure. According to the Second Law of thermodynamics, the Gibbs free energy of

a solution in a state of thermodynamic equilibrium should be at a minimum with respect to any free parameters. Assume a dilute solution of sticky-edged building blocks, such as the truncated triangular pyramids of the previous section. We will call them "particles". Let $C(n)$ be the concentration of an n-particle aggregate with $n = N >> 1$ the assembled capsid. The Gibbs free energy of a dilute solution of aggregates of all sizes is:

$$G/V \sim \sum_{n=1}^{N} \{E(n)C(n) + k_B T C(n) (\ln C(n)/\phi_0 - 1)\} \tag{1}$$

Here, $E(n)$ is the cohesive free energy of an n-particle cluster with $E(n=1) = 0$ and ϕ_0 is an undetermined constant. Minimizing G with respect to $C(n)$ under the constraint that the total particle concentration $\sum_{n=1}^{N} nC(n) = \phi$ is fixed leads to

$$C(n)/\phi_0 = \exp -\beta [-\mu n + E(n)] = (C(1)/\phi_0)^n \exp -\beta E(n) \tag{2}$$

The Lagrange multiplier $\mu = k_B T \ln (C(1)/\phi_0)$ was used to impose the constraint, It can be identified as the *chemical potential* of the particles. The resulting relation is known in physical chemistry as the Law of Mass Action (LMA) . By measuring $C(n)$ one could — in principle — measure the complete free energy spectrum $E(n)$ of n-particle clusters (such measurement are done by methods like Size-Exclusion Chromatography[3]).

First assume the simple case that the concentration of clusters with $1 < n < N$ is negligible, so only single particles (n=1) and assembled capsids (n=N) are appreciable. The two corresponding concentrations are related by $\phi \simeq C(1) + NC(N)$. Together with Eq. 2, there are then two equations for the two unknowns $C(1)$ and $C(N)$. After solving for C(1) and C(N) one finds that for $N >> 1$ there should be practically no capsids for ϕ less than a threshold concentration $\phi^* = \phi_0 \exp (E(N)/(Nk_B T))$. At this point the chemical potential μ for the particles in solution equals the binding energy $\varepsilon(N) = E(N)/N$

[3] A gel filtration technique that separates molecules and their aggregates according to size or molecular weight. See, for example, [18].

of a particle as part of a shell (for the closely analogous case of micelle formation by lipids, ϕ^* is known as the "Critical Micelle Concentration" [7]). On the other hand, for ϕ larger than ϕ^*, the fraction $f(\phi)$ of particles that are part of a capsid rises with ϕ as $f(\phi) \simeq 1 - \frac{\phi^*}{\phi}$. One can formally view ϕ^* as the critical point of an equilibrium *phase transition*. Finally, we can crudely estimate the constant ϕ_0 for our case by noting that for $E(N)$ smaller than k_BT, capsids should be unstable against thermal fluctuations until the particle concentration is so high that capsids can be stabilized by close-packing. From this condition we estimate that $\phi_0 \sim N/R^3$ with R the radius of the capsid.

The agreement between these predictions and chromatography studies of the self-assembly of CCMV [18] and other viruses is excellent. The concentration of assembly intermediates is indeed negligible. From the single fitting parameter: ϕ^* one obtains an estimate for the cohesion energy $-E(N)$ of a capsid. For CCMV, $-E(N)$ is found to be of the order of 10^3 times the thermal energy k_bT. That means that $\varepsilon(N)$, the binding energy per CP, must be in the range of 3-5 k_BT. This surprisingly low value means that thermal fluctuations must play an important role during viral assembly, with many forward and backward steps, as is confirmed by simulation studies [11, 12, 13].

So why is the concentration of intermediate-sized protein clusters negligible? It follows from Eq. 2 that for $\phi \sim \phi^*$ the relative concentration of *half-formed clusters* can be estimated as $C(N/2)/C(N) \sim \exp -\beta(E(N/2) - E(N)/2)$. The difference $2E(N/2) - E(N)$ is the *scission energy*, the free energy cost of breaking a capsid up into two equal sized hemi-spheres. If the characteristic energy scale $\varepsilon(N)$ for the bond between two particles is a few k_BT then for $N \sim 100$ the scission energy is in the range of tens of k_BT. That means that the concentration of hemispherical assembly intermediates indeed should be negligible compared to that of fully assembled capsids.

3.2 The Equilibrium Assembly of Caspar-Klug Icosahedra

It is easy to assemble a T=1 capsid from twenty triangular protein units. However, the assembly of shells with larger T is not so simple: how do you know when to insert one of the twelve pentamer along the rim of a growing shell? Numerical simulations show that assembly of larger T-Number shells requires delicate fine-tuning of the shape of the building blocks [13]. Even then the yield is low: many assembly events produce malformed structures. One suggestion is that the CPs could have a complex spectrum of internal states that are "programmed" to facilitate the assembly process [19]. Alternatively, if the Caspar-Klug icosahedral shells would the minimum free energy structures of aggregates of CPs then, provided the kinetics is not too slow, annealing by *thermal fluctuations* should produce the Caspar-Klug structures. What sort of structural fine-tuning is required of building blocks for that to happen, assuming that there is no complex spectrum of internal states?

The hexamers and pentamers of Fig. 1 are roughly circular. Many larger viruses assemble on spherical surfaces, which are known as "scaffolds". As a naive model of capsid assembly, one could think of the hexamers or pentamers as circular disks with attractive edges placed on a spherical surface. Assume N circular disks are placed on the surface of the scaffold sphere and that the radius of the sphere is reduced to its smallest possible value. The close-packed N-disk structure should correspond to the minimum energy structure of a shell composed of N sticky disks. Finding these structures is known as the "Tammes problem", after a Dutch botanist who studied the structure of pollen particles. Tammes structures exhibit a variety of interesting symmetries [20] but, sadly, the Caspar-Klug icosahedra are not among them.

Let's make the model a bit more realistic by distinguishing hexamers from pentamers by representing them as two different types of particles — denoted by H and P — that

again condense on the surface of a scaffold sphere. Let the H and P particles interact via a Lennard-Jones (LJ) interaction where the repulsive part of the LJ potential represents the resistance of hexamers and pentamers against compression while the attraction represents the hydrophobic attractive interaction between hexamers and pentamers minus electrostatic repulsion. H-H, P-P and H-P particles interact via LJ potentials that have different minimum energy separations. The choice of the minimum energy spacing is determined by the geometrical construction shown at the top of Fig. 5. Because the hexagons and pentagons of the CK construction have the same edge length, the ratio of the radii of the circles that circumscribe pentamers and hexamers is 0.93 and the equilibrium spacings between H and P particles are chosen to correspond to this ratio. The depth of the LJ potential ε_0 between particles should be in the range of $10k_BT$ for the cohesive energy of a completed shell of 100 particles to be in the range of $1000k_BT$.

Place again N of these particles on the surface of a sphere and allow the system to evolve towards a minimum free energy state, for example by Monte-Carlo simulation, allowing H and P particles to switch identity (an HP chemical potential difference can be included). The energy $E(N,R)$ of this N-particle system is then minimized with respect to R in order to optimize the choice of R. Figure 5 shows $\varepsilon(N) = E(N)/N$. Recall that the onset-concentration for capsid self-assembly from solution is determined by the condition that the chemical potential $\mu(\phi)$ of the building blocks of the capsid equals $\varepsilon(N)$. It follows that the *minima* of the curve $\varepsilon(N)$ should correspond to the shells that are formed as the concentration of particles in solution is raised. The plot of $\varepsilon(N)$ is quite jagged. The lowest minima are near certain "Magic Numbers": N=72, 42, and 32. Self-assembly from solution thus should produce predominantly these structures when the chemical potential of the components in solution are increased. The minimum energy structures are shown in Fig. 5. It turns out that each of these structures has exactly twelve

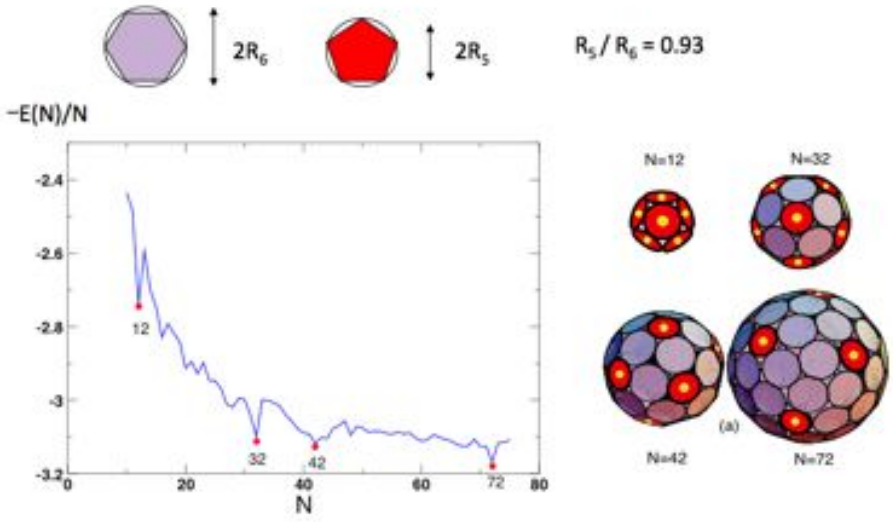

Figure 5: Left panel: Capsid energy per particle $\varepsilon(N)$ as a function of the number of particles. From [21]. Right panel: minimum energy structures. They correspond to the T=1, 3, 4, and 7 Caspar Klug icosahedra.

P particles and that they are in fact the T=7, T=4, and T=3 Caspar-Klug icosahedra with 72, 42, and 32 hexamers plus pentamers.

What determines whether a T=3, a T=4 shell, or a T=7 shell emerges? Hexagonal sheets of capsid proteins have a *spontaneous curvature* due to the lack of up-down symmetry of the capsid proteins (see Fig. 2A) [17]. Let the preferred curvature radius be R^* and include a global "bending energy" term of the form $(1-R/R(T))^2$ that has a broad minimum at a preferred curvature radius $R=R(T)$ roughly in the neighborhood of a T-number shell. The sharp minima of $\varepsilon(N)$ at the magic Numbers then assures us that only that T-number shell will form as the solution concentration of the particles increases. In summary, provided CPs have the ability to form pentamers and hexamers and provided a hexagonal sheet of CPs has preferred curvature radius that is roughly in the right range then the Caspar-Klug icosahedron of choice will assemble. It is not necessary to require the CPs to be programmable. This of course does not explain *why*

the T-number structures are so prevalent among viral shells, but that is a question of evolutionary microbiology.

3.3 The Next Level: Self-Assembly Mark II.

Classical equilibrium assembly theory seems to describe successfully *in vitro* capsid assembly studies, but there is a problem. Neither the cytoplasm of our cells nor the extracellular fluid surrounding our cells carries, under normal conditions, many free-floating CPs. In an equilibrium description, viruses should disassemble under these conditions, which — unfortunately — they do not: virus assembly is clearly an irreversible process. The *in-vitro* assembly experiments of empty capsids actually show hysteresis and irreversibility as well [22]. If, for example, the CP concentration is reduced back down to below ϕ^*, then capsids should disappear. This, again does not happen [4].

The mechanism behind the exceptional stability of viral capsids, as compared with traditional self-assembled equilibrium structures composed of amphiphiles, can be illustrated by an elegant model for capsid assembly due to Zlotnick [23] where the capsid is a dodecahedron assembled from twelve regular pentamers with sticky, slanted edges. There are many different assembly pathways to fit twelve pentamers together to form a dodecahedron but if one maximizes the binding energy of an n-pentamer partial shell for each n, then the assembly pathway is unique, apart from trivial degeneracies. This pathway is illustrated in Fig. 6: Let ε be the edge-to-edge binding energy between two pentamers. Figure 6 gives the energy gain $E(n+1)-E(n)$ when a pentamer is added for each successive step. The average energy gain for the intermediate steps is about 2.5ε with only a modest variation around the average. However, the energy gain of the very

[4] In order to re-dissolve self-assembled capsids it is necessary to change thermodynamic conditions, for example by increasing the pH

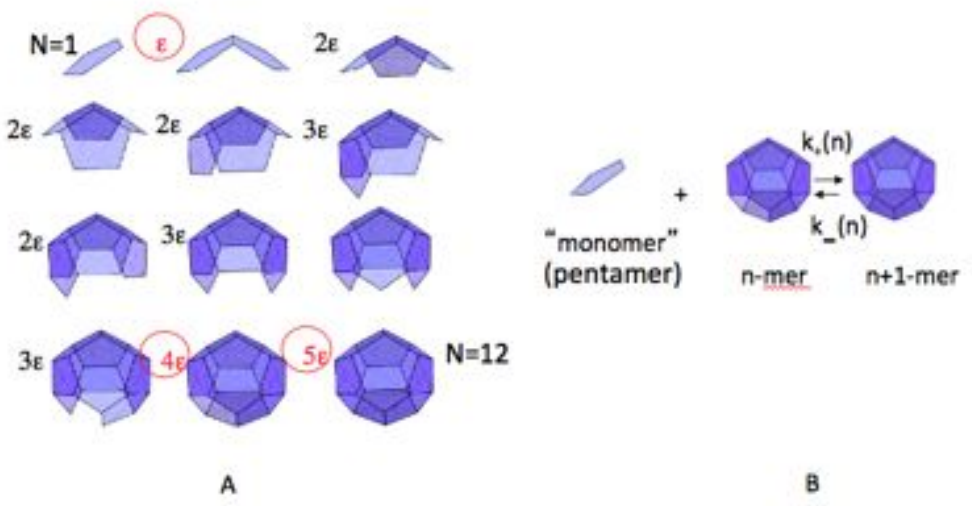

Figure 6: A) Assembly path of a dodecahedral virus constructed from sticky-edged pentamers. From [18]. The cohesive energy gain of each step is indicated. Exceptional cases are circled. B) Forward and backward rates of n'th step of the assembly process written in the form of a polymerization chemical reaction

first step is less, only ε, while the energy gain of the last two steps, the "closure" of the shell, together equals 9ε. Let's take ε to be $3k_BT$, based on the equilibrium assembly studies discussed above. Then $2.5\varepsilon \sim 7.5k_BT$ and $9\varepsilon \sim 27k_BT$. The initial "nucleus" for capsid assembly — two pentamers — is thus rather unstable, the intermediate states are more stable, while the final closure of the capsid involves binding energies so large that capsid disassembly by thermal fluctuations may not take place on laboratory time-scales. The assembly of the dodecahedon can be viewed as an eleven step random walk along the optimal assembly pathway linking the first and last state.

As a simple generalization, assume a capsid composed of N capsomers that has a unique N-1 step minimum energy assembly pathway. The energy gain ΔE for adding one capsomer is now assumed the same for all assembly intermediates. The exceptions

are the last step – closure – for which the energy gain is assumed infinite and the first step – nucleation – for which the energy gain ΔE_0 is less than ΔE. Finally, the "on-rate" k^+ for adding a capsomer is independent of n, which corresponds to the limit of low CP solution concentrations where transport is diffusion limited. This model is analytically tractable [24] by the methods of random-process theory [25]. Define C(n,t) to be the time-dependent concentration of a partial shells composed of n capsomers and define the assembly current $J(n,t)$ to be the net rate at which n-mers are transformed into n+1 mers at the nth step. The assembly current then can be expressed as the difference between an assembly and a disassembly term:

$$J(n,t) = k^+ C(1,t)C(n,t) - k^-(n)C(n+1,t) \tag{3}$$

with $k^-(n)$ the disassembly or "off-rate" and k^+ the on-rate. Because the number of capsomers in solution is conserved, there is a conservation equation for each site of the assembly pathway:

$$\frac{\partial C(n,t)}{\partial t} = J(n-1,t) - J(n,t) \tag{4}$$

which is the *Master Equation* of the stochastic process. It must be solved under the constraint $\sum_{n=1}^{N} nC(n) = \phi$. Under conditions of thermal equilibrium *all* currents $J(n,t)$ must be zero because of *time-reversal symmetry*, the condition of Detailed Balance. The set of conditions $J(n,t) = 0$ should be consistent with the equilibrium cluster size distribution $C(n) \propto \exp(-\mu(\phi)n + E(n))$ discussed in the previous section. For the intermediate steps, this leads to

$$k^-/k^+ = \phi_0 e^{\beta \Delta E} \tag{5}$$

independent of n. The exception is the off-rate rate for the dimer state $k^-(1)/k^+ = \phi_0 e^{\beta \Delta E_0}$, which is higher. In the continuum limit of large N, the Master Equation reduces

to a variant of the Advection-Diffusion Equation [5]:

$$\frac{\partial C(n,t)}{\partial t} = V(t)\frac{\partial C(n,t)}{\partial n} + D(t)\frac{\partial^2 C(n,t)}{\partial n^2} \tag{6}$$

Here, $V(t) = (k^+C(1,t) - k^-)$ is the *assembly velocity* while $D(t) \simeq 1/2(k^+C(1,t) + k^-) + ..$ acts as a *assembly diffusion coefficient*. The capsomer concentration C(1,t) must obey the self-consistency condition $C(1) + NC(N) + \int_{n=2}^{N-1} nC(n) = \phi$. The rate equations for C(1,t) and C(N,t) must be maintained separately in their discrete form (see Eq.4). e.g. $\frac{\partial C(1,t)}{\partial t} = -k^+C(1,t)^2 + k^-(1)C(2,t)$ from which it follows that if the dimer breakup rate $k^-(1)$ is high then the monomer concentration $C(1,t)$ decreases only slowly.

Assume that at time t=0 there are only monomers in solution with concentration ϕ. If $\phi > k^-/k^+$, then a *shock front* emerges in configuration space at n=1 that moves with a – time-dependent – velocity $V(t)$. Because of the diffusion term, the shock front becomes more rounded in time. After the shock front has reached N, capsid assembly starts. The "waiting time" is thus of the order of $N/(k^+\phi - k^-)$. The advection velocity V(t) diminishes with time as the monomer supply is depleted and stops when $C(1) \simeq k^-/k^+$ when $V \simeq 0$ and $D \simeq k^-$. The Master Equation thus reduces to the diffusion equation, a much slower form of transport as compared to front propagation. The assembly intermediates are now in a state of quasi-equilibrium with respect to the monomer concentration and this stifles capsid assembly, apart from the residual diffusion current. If the front stops before reaching N, then this corresponds to a case where many partial capsids form but few completely assembled shells. This happens when the dimer disassembly rate $k^-(1)$ is decreased significantly, which increases the magnitude of the assembly current.

The fraction of capsomers in capsid form in this quasi-equilibrium state is approximately $f(\phi) \simeq 1 - C(1)/\phi$. This expression has the form of the Law of Mass Action if one identifies $C(1)$ with the CMC. If one compares $C_(1) \simeq k^-/k^+ \simeq \phi_0 \exp \Delta E/k_B T$

[5] see Advective Diffusion Equation, lecture notes by Scott A. Socolofsky and Gerhard H. Jirka

with the actual CMC $\phi^* = \phi_0 \exp E(N)/(Nk_BT)$ then one sees that the quasi equilibrium state obeys the Law of Mass Action for a *fictitious* capsid with $E(N)/N = \Delta E$. Numerical solution of specific models reach the same conclusion [22]. Assembly shock fronts have been seen as well in simulations [26]. Measurements of $C(N,t)$ by Small-Angle Light Scattering [27] for papillomavirus assembly kinetics are also consistent with the "quasi-reversible assembly-line" model outlined here. If correct, this means that the free energies measured from chromatography studies do give us information about the energetics of the intermediate reversible states, but not about the total capsid free energy.

From the viewpoint of material science, this hybrid form of assembly can be viewed as a brilliant improvement on equilibrium self-assembly. Just as for equilibrium assembly, the intermediate reversible assembly steps allow for a "cautious" assembly where the modest energy gain per step allows for reverse steps, and hence for the correction of the assembly errors as discussed below. But unlike equilibrium assembly, the final irreversible step (or steps) that complete(s) assembly prevent destruction of assembled capsids by thermal fluctuations when the concentration of assembly units in solution goes to zero.

3.4 The Death of a Traveling Pathway and Entropic Stabilization.

It would seem that a minimum-energy assembly pathway provides a royal road for error-free, irreversible assembly of robust viral shells. Natural selection surely must have produced such a pathway for every viral shell. Or has it? The assembly of small capsids does appear to be guided by minimum energy pathways. However, both experimental[28] and numerical [29, 30] studies of the assembly of small capsids indicate that the minimum energy pathway actually has *side-branches*, dead-end streets in the form of aberrant, malformed structures that act as *kinetic traps*. Numerical simulations of the simple mod-

els that include all possible ways of putting the building blocks together [29, 30] show that the effects of kinetic traps become more noticeable as the assembly velocity V(0) of the last section increases and also as the complexity of the structure increases. Natural selection appears to have minimized the effects of side-branching for the assembly of small viruses but it has certainly not succeeded in eliminating them altogether, which would appear to be mathematically impossible.

As the size of the capsid increases, the very concept of a minimum-energy pathway starts to break down. Construct a large shell by adding hexamers one-by-one along the rim of a growing circular nucleus. In the next section we will discuss that, with certain restrictions, large shells can be described by *continuum elasticity theory* and we can apply it to the growing nucleus. Recall that sheets of CP hexamers have a spontaneous curvature so the nucleus will starts to curve in, which generates *elastic stresses*. To be specific, consider a 12 hexamer nucleus of a T=13 shell centered at a 3-fold symmetry site (see Fig. 7. This is the point where it is necessary to insert pentamers if one wants to construct a T=13 shell. It in fact follows from continuum elasticity theory that the curvature-induced elastic energy of the nucleus can be reduced by inserting pentamers. Could the release of elastic stress determine a minimum energy pathway for the assembly of a T=13 shell ? Figure 7 shows the elastic energy of the twelve-hexamer nucleus [31] with the preferred curvature set equal to that of a T=13 shell. The elastic energy of each hexamer computed numerically is indicated (in arbitrary units). The elastic moduli were given values that would be consistent with those measured by micromechanical means. In order to end up with a T-13 shell, three equidistant pentamers must now be inserted along the rim. However, Fig. 7 shows that when a pentamer is inserted there is a large increase of the elastic energy of the adjacent hexamers Inserting a ring of pure hexamers would in fact be the minimum energy pathway at this stage of assembly,

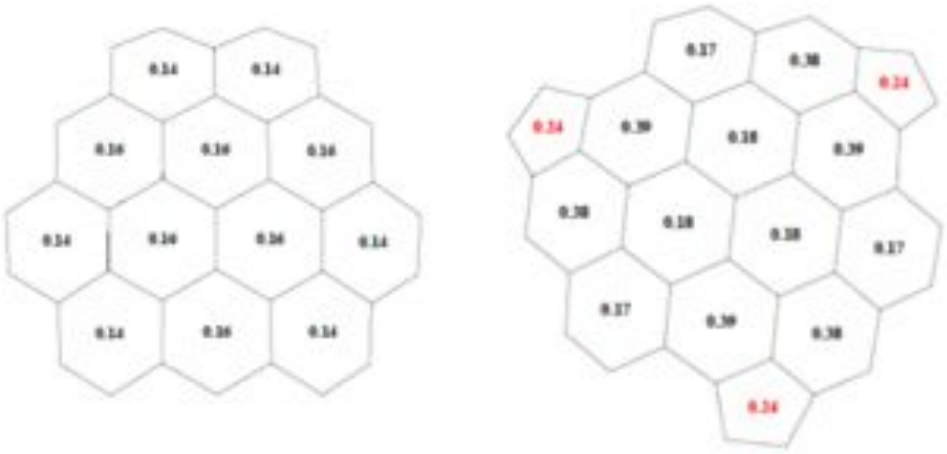

Figure 7: Growth nuclei of a T=13 shell. The energy of the nucleus is computed from continuum elasticity theory. The elastic energy of individual capsomers is indicated (arbitrary units). Left panel: twelve hexamers. Right panel: three pentamers are added as required for a T=13 shell. The elastic energy of the hexamers adjacent to the pentamers is strongly increased.

so T=13 shells could not form. For no reasonable value of the elastic parameters is it possible to have the pentamers correctly inserted. This resut is not a result specific to this particular model. In continuum elasticity theory, pentamers acts as *5-fold disclinations*. Disclinations are attracted by a strong *image force* to free boundaries where they would be expelled, preventing pentamer insertion. In short, according to continuum elasticity theory there is no no minimum-energy assembly pathway for large shells. Simulations of the assembly kinetics of larger shells [32] reveal that a variety of additional growth instabilities appear, such as "closure catastrophe" and "hole implosion". They are related to growth instabilities encountered in condensed-matter physics, such as the Mullins-Sekerka instability [33] and the Asaro-Grinfeld-Tiller instability [34]. The combined effect of all of this is a wild proliferation of defects during the later stages of assembly

[32]. There is no royal road for the assembly of large viruses. Very similar problem are encountered in the growth of crystals with large, complex unit cells, such as quasi-crystals[35].

How can larger viruses assemble if there can be no minimum energy pathway? There appear to be two options. The first is that the CPs are clever nano-computers with a complex spectrum of internal states that do the necessary computations to decide when and where to insert [19]. It is not obvious that this is physically even possible but, anyway, there currently is no evidence for the existence of such CP-devices. The second is that CPs are not clever but that *thermal annealing* transforms disordered shells into the Caspar-Klug icosahedra if these are the minimum free energy states. The success of this transformation would be guaranteed by the Second Law of Thermodynamics, though it might be quite slow. In this view, Caspar-Klug icosahedra are *entropically* stabilized during and following growth. Entropic stabilization may well explain the growth of quasi-crystals [35]. If entropic stabilization is the assembly route that nature follows for large viruses, then the capsids of large viruses *in their initial state* must be sufficiently fluid to allow for the transport of pentamers during annealing. The irreversible steps at the end of the viral assembly process discussed above are, in this view, postponed till *after* the formation of the Caspar-Klug shell. These irreversible steps may have to be quite drastic. Some large viral capsids act as pressure vessels capable of withstanding pressures in the range of tens of atmospheres. These pressures could not possibly be absorbed by thermally equilibrated capsids with interaction energies in the range of a few k_BT. Such a reinforcement process — which is irreversible — is a form of *maturation*, which indeed is commonly encountered in viral assembly, as we will now discuss.

4 A Structural Mechanics for Capsids

In the previous section we focused on descriptions of viral capsids at larger length scales, without paying attention to the capsid proteins and their mutual interactions. We mentioned that the spectrum of internal states of a protein and the effect of interactions between proteins might play a role during assembly and, in general, should be an integral part of a description of the physics of a capsid. In principle, the physical mechanisms governing capsid conformation could be understood with all-atom molecular dynamics modeling. While such simulations are increasingly within feasible range with modern computing resources, especially for small viruses such as CCMV and other $T = 3$ viruses [36], molecular models introduce challenges of their own, including (a) the need to interpret the results of large datasets from dynamic trajectories, and (b) the difficulty of extracting general principles from molecularly specific models. These issues are compounded when posing the question of how conformational deformation is managed (or even utilized) for viruses with *large* T-numbers, many of which can exhibit large conformational changes during the *viral maturation* processes we just mentioned. (Fig. 8)

In this section, we explore a different approach based on *continuum elasticity*. It is by no means obvious that continuum theory is applicable, given the relatively large size of the molecular components — the CPs — with respect to the that of the capsids. We will see that there are indeed fundamental obstacles in the applications of conventional continuum theory to viral capsids, in particular during maturation processes, and we will discuss the development of a new form of elasticity theory designed to overcome these obstacles.

As before, we construct capsids from a flat hexagonal sheet, but we now place six "real" CPs on the hexagons and allow them to bond forming a two-dimensional (2D) crystal with hexagonal symmetry where all protein locations are symmetry-equivalent.

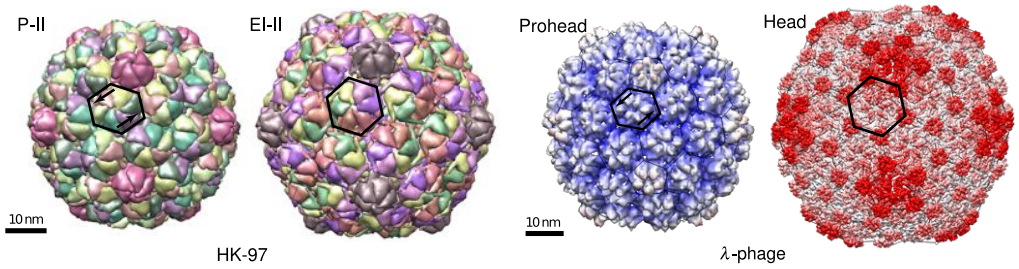

Figure 8: Many viruses assemble into an initial "prohead" conformation and subsequently "mature" by undergoing large conformational changes. (Left) For bacteriophage HK97 the transition from the prohead "P-II" state to the expansion intermediate "EI-II" state involves unshearing of skewed hexamers to symmetric conformations. (Right) The maturation of bacteriophage λ from prohead to head state exhibits a similar symmetrization of skewed hexamers. Coordinates obtained from ViperDB [37] and EMDB [38] and rendered in Chimera [39].

The proteins adopt a configuration that corresponds to the minimum free energy state of the 2D crystal. We will treat this 2D crystal as the *stress-free reference state*. Now, carry out a CK construction on this 2D crystal to produce a T-Number icosahedron. Only for a T=1 shell will all proteins remain in symmetry-equivalent locations, with three proteins per equilateral triangle. For general T, there are T inequivalent protein locations . The physical interactions among proteins in different symmetry environments are necessarily different as well. The minimum free energy configuration of the protein molecule cannot be simultaneously compatible with assembly into the T distinct symmetry environments of the shell. It follows that there must be some conformational deformation of the proteins away from the minimum free energy state to accommodate the incompatibility. The assembled structure is thus determined not purely by the CK geometric principles, but also by the physical principle of free energy minimization that reflects a balance of forces produced by the stretching of the (non-covalent) bonds holding the

shell together. In other words, the protein lattice is *strained*.[6]

High-resolution X-ray structures have shown that capsid proteins indeed take on different conformations depending on their locations. One possibility is that these conformational variants "pre-exist" as (metastable) local free energy minima of isolated proteins, as envisioned in the local-rule model [19]. For example, the *isolated* capsid proteins of a $T = 3$ virus could undergo switching among the three conformational states A, B, and C. Alternatively it could be that these three states are, in effect, only generated by the (quaternary) interactions with neighboring subunits as established during assembly.

4.1 A "Classical" Theory of Elasticity for Viral Shells

A significant step forward in understanding the connection between protein conformation and capsid mechanics came from examining the $T \to \infty$ mathematical limit of the CK construction by Lidmar, Mirny, and Nelson [40] (LMN). In effect, LMN assumed that proteins have no internal states and can be treated as pieces of homogeneous elastic material, as we did at the end of last section. LMN introduced an elastic shell theory for capsids by taking the equilateral hexametric lattice as the *stress-free reference configuration* of a sheet of these elastic capsid proteins. Recall that the CK construction was achieved by aligning a hexagonal sheet with an unfolded flat template for an icosahedron such that so that icosahedral vertices are connected by integral steps h and k along the hexamer lattice basis vectors (see Fig. 3). Trimming along the boundaries of the icosahedral template removes a wedge of angle $\pi/3$ from each of the capsomers positioned over an icosahedral vertex. As the template is folded along its edges (green

[6] Caspar and Klug argued that the CK construction represents a minimal deviation from perfect symmetry equivalence between proteins, and introduced the term "quasi-equivalence" to describe this.

in Fig. 3), the joining of adjacent boundary edges leads to the Volterra construction of five-fold *disclinations* at each of the 12 icosahedral vertices. In the LMN approach, the pentamers are transformed into topological defects of the hexagonal lattice. The folding of the sheet along icosahedral edges allows the formation of a closed shell from a flat sheet in a locally *isometric* way, i.e., without any local stretching of the sheet. Equilateral triangles remain equilateral triangles. A CK icosahedron has sharp folds connecting the twelve vertices. For an elastic sheet of finite physical thickness, the elastic energy cost induced by bending deformations is, to lowest order, a quadratic function of the local principal radii of curvature, and can be expressed in terms of the *mean curvature* $H = 1/2(1/R_1 + 1/R_2)$ and *Gauss curvature* $K = 1/R_1R_2$ — with $R_{1,2}$ the principal radii of curvature of the surface — as

$$\mathscr{F}_{\text{bend}} = \int dA \left(\tfrac{1}{2}\kappa(2H)^2 + \kappa_G K\right).$$

Micromechanical studies of capsids [41] indicate that the mean bending modulus $\kappa \sim 10 - 100 k_B T$. (The classical derivation from 3-D elasticity theory gives $\kappa_G = (\nu - 1)\kappa$, suggesting a similar order of magnitude if the Poisson ratio ν in the typical range $0 \leq \nu \leq 0.5$.) Accordingly the (infinite) curvature produced by folding along icosahedral edges will generally be relaxed over larger length scales, which can only be accomplished though some in-plane stretching of the sheet. The energy of this in-plane stretching is, to lowest order, quadratic in the strain tensor u_{ij}

$$\mathscr{F}_{\text{stretch}} = \int dA \tfrac{1}{2}\left(\lambda (u_{kk})^2 + \mu u_{ij} u_{ij}\right),$$

where the elastic Lamé coefficients λ and μ are related to the 2-D Young's modulus Y and Poisson's ratio ν as $\lambda = \frac{Y}{(1-\nu^2)}$ and $\mu = \frac{Y}{2(1+\nu)}$. To account for the coupling between bending and stretching deformations it is essential to include the nonlinear dependence of strain on the displacements of the surface, which to lowest order gives $u_{ij} = \frac{1}{2}(\partial_i u_j +$

$\partial_j u_i + \partial_i f \partial_j f$) for displacement components $\{u_1, u_2\}$ in the reference plane, and $u_3 = f$ in the normal direction. For open sheets, Seung and Nelson [42] found that disclinations drive a bifurcation-type buckling instability when the Föppl-von Kármán number, $\gamma = \frac{YR^2}{\kappa}$, a ratio of stretching to bending moduli normalized by sheet radius R reaches a critical value of ≈ 150. For γ subcritical, bending stiffness dominates and the sheet stretches to remain flat. As γ increases above the critical point the sheet will buckle out of the plane. Five-fold disclinations, like those at the vertices of the icosahedron, drive sheets to buckle into conical shapes. For closed icosahedral shells this buckling transition is manifest in the asphericity of the shell. As the FvK number increases above a value of $\gamma \approx 250$ the shell shape transitions rather abruptly from spherical to facetted, with the icosahedral vertices buckling radially outward (see Fig. 9).

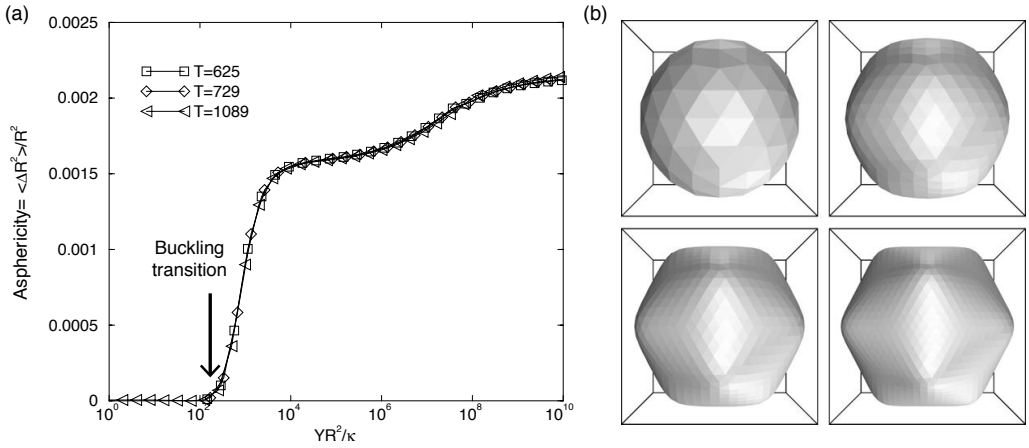

Figure 9: The buckling transition for icosahedal and asymmetric elastic shells. Adapted from [40].

These predictions of elasticity theory turn out to be consistent with a trend that can be observed in X-ray and CryoEM structures — larger capsids tend to be more facetted than smaller capsids. The theory has also found agreement [43] with coarse-grained molecular models [44] in identifying the buckling transition as a soft mode of mechanical de-

formation for icosahedral viruses. Likewise the theory has been extended to explain the formation of spherocylinder and conical capsid shapes [45], capsid polymorphism [46], and the nonlinear mechanical response under atomic force microscopy (AFM) loading [47] (for a review, see [41]).

4.2 A Mechanics Theory for Active Capsids

Despite these successes it is clear that something fundamental is missing from the narrative provided by thin-shell elastic theory: proteins are *functional* structures with internal "gears" and "wheels", the above-mentioned internal states. Viral capsids are in fact not merely passive containers but macromolecular machines able to perform specific tasks associated with protein conformational changes [48]. These issues are well illustrated by the case of HK97, where insertion of the viral genome molecule into the capsid triggers a complex sequence of conformational changes, an example of the earlier-mentioned maturation, that progressively strengthen the shell against the large internal pressures exerted by the tightly packaged genome [48]. The sequence initiates with the "P-II to EI" transition [49, 50, 51] (see Fig. 8). Cryo-EM pictures of HK97 show that this transformation is marked by both a buckling-like transition in capsid shape from spherical to polyhedral and a change in the shapes of the hexons from skewed or "twisted" to symmetric (Fig. 4). Detailed X-ray reconstructions reveal that the transformation is driven by the release of elastic energy, stored in the highly deformed hexons [52, 51]. At a later stage of maturation, a spherical structure reappears. Many other viruses go through similar maturation sequences involving both local skewing of capsomers and global changes in morphology [53, 54, 55, 56, 57]. The LMN theory would require an interpretation of such events as being based on changes in the effective mechanical properties (Y and κ) of the protein shells, perhaps linked to changes in the effective thickness or bonding

structure due to the conformational changes. However, thin shell theory simply cannot account for the observed displacements of the capsid proteins during maturation, such as the fact that for HK97 the hexamers commonly take on skewed shapes in the initial prohead configuration and are made symmetric in the final head configuration (Fig. 8). Moreover, observed relative displacements of the capsid proteins are much too large to be compatible with elasticity theory. This failure is puzzling given the fact thin shell theory explains a number of observations made on the mechanics of capsids.

These puzzles are related to deeper questions about the use of condensed-matter physics and elasticity theory in describing protein aggregates in general. The most obvious question is whether continuum theory could reasonably be expected to apply at length scales of the size of a capsid protein or of a protein hexamer/pentamer. Elastic network models are actually quite able to describe *small* deformations of proteins down to length scales of a few nm, provided proper account is taken of the heterogeneous structure of proteins. The more fundamental concern is the identification of the *stress-free reference state* of protein aggregates. In the LMN theory, the stress-free reference state is, by assumption, a hexagonal sheet. For the case of HK97, structural studies reveal locally asymmetric (i.e., skewed) capsomers that simply cannot be assembled into a flat hexagonal sheet. More generally, the irregular, asymmetric shape of a protein in general need not be *geometrically compatible* with the final assembled shell. The internal forces holding together the assembly necessarily deform the units, inducing internal residual stresses. This problem is accerbated when conformational transitions of proteins produce large displacements and deformations that are *discontinuous* across protein-protein interfaces, as is the case for HK97; motions that will further modify the state of residual stress in the assembly. In short, LMN theory identifies only *one* of the two sources of intrinsic stress of a viral capsid, namely the one due to the incompatibility between a

hexagonal sheet and a closed shell. The second source of intrinsic stress derives from the incompatibility between the minimum energy structures of asymmetric protein aggregates and the geometry of a closed shell. We now will discuss a generalization of elasticity theory that incorporates these "incompatibility stresses of the second kind".

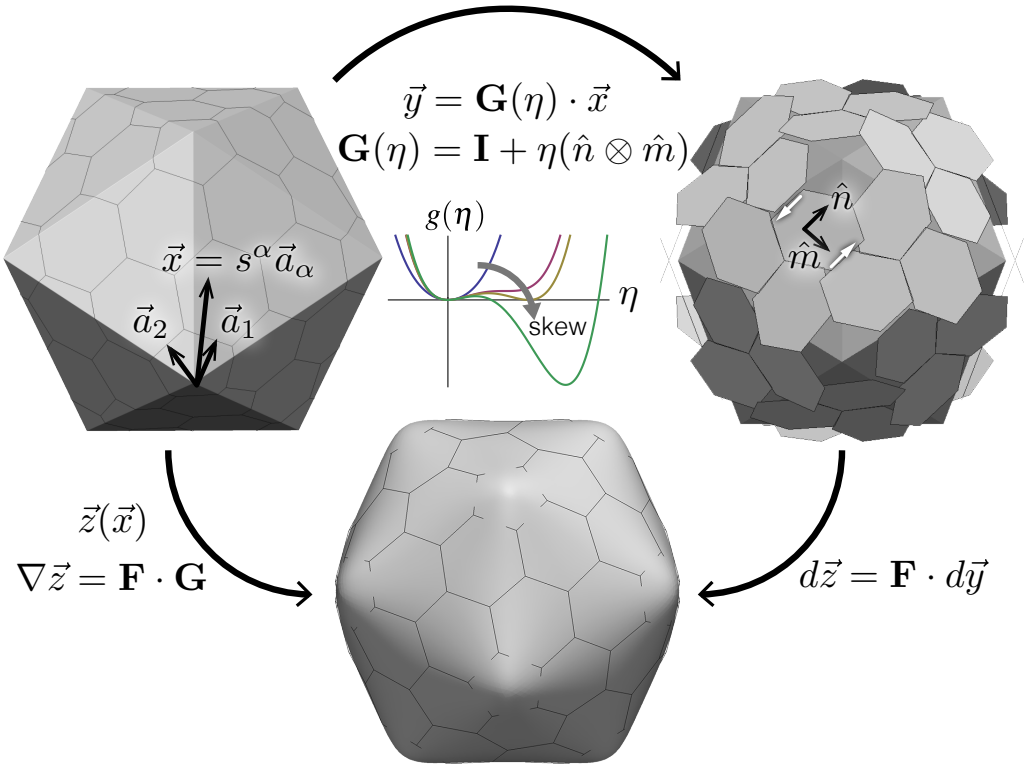

Figure 10: Conformational skewing of hexamers breaks the CK construction. The maturation process can be modeled by a Landau theory in which the conformational strain order parameter η is coupled to shell mechanics through the elastic deformation gradient $\mathbf{F}$, which restores the integrity of the shell broken by incompatible hexamers shear $\mathbf{G}(\eta)$.

4.3 A Viral Martensite

We need to re-examine the very foundation of elasticity theory: the assumption of a *stress-free reference configuration* and apply the concept of *structural phase transitions*

from condensed matter physics [58] to viral shells [59]. The symmetric and sheared conformations of HK97 can be viewed as analogous to, for example, the austenite and martensite phases in iron-carbon alloys. We will borrow from condensed matter physics the concept of the *Bain strain* [58]. In our case, this is an affine transformation of the position $\vec{x}$ of a material point in the symmetric hexamer reference configuration, to a point $\vec{y} = \mathbf{G} \cdot \vec{x}$ in the asymmetric hexamer state. The conformational deformation gradient tensor $\mathbf{G} = \mathbf{I} + \eta \hat{n} \otimes \hat{m}$ represents an area-preserving shear of magnitude η along the direction of unit vector $\hat{m}$, in local Cartesian frame $\{\hat{m}, \hat{n}\}$. The lower-symmetry skewed units in the $\vec{y}$ configuration can tile the plane with a uniform shear orientation $\hat{m}(\vec{x}) = \text{const}$. The CK construction of an icosahedral shell, however, requires that the units be oriented according to the icosahedal group. This constraint breaks geometric compatibility, and requires that the lattice units undergo some additional elastic strain to assemble into a continuous shell.

The case for an analogy with structural phase transitions is strengthened further by the observations that the conformational motions in maturation represent *soft modes* of the capsid structures [60, 44, 61]. Widom, Lidmar, and Nelson [43] showed that the radially dominant displacement patterns of the buckling transition of icosahedral shell theory are closely matched with the lowest frequency elastic normal modes of the shell. However this is only part of the story told by more detailed molecular models, which show that even the conformational motions parallel to the shell surface (sliding and twisting of subunits, e.g., the hexamer skewing in HK97) are strongly reflected in the low frequency icosahedral modes. This suggests that these conformational motions act like special degrees of freedom, internal coordinates or mechanisms, that couple to the elasticity of the shell on larger lengths scales.

4.4 A Landau Theory for the Structural Mechanics of Viral Shells

The natural framework to describe the coupling between internal degrees of freedom and macroscopic strain is by Landau theory [59]. Construction of a Landau theory for capsid maturation starts by identifying the appropriate symmetries of the field variables. HK97 has multiple soft modes, which in principle should be included in a Landau description, but we will restrict ourselves here to the Bain strain as the sole order parameter. This is a rank-two second-order tensor with unit determinant, tracked by the scalar shear magnitude $\eta(\vec{x})$, to which we attribute a Landau energy $g(\eta)$. Because maturation events involve large displacements, the description of the elastic deformations is now more involved, requiring the machinery of large-deformation, nonlinear elasticity on curved surfaces. We can track the motion of material points using the lattice vectors $\hat{a}_\alpha$ in the CK hexagonal sheet, defining reference positions $\vec{x} = s^\alpha \hat{a}_\alpha$ (employing the Einstein convention), with (s^1, s^2) acting as convected curvilinear coordinates on the shell surface. For each hexagon i in the reference sheet we define the conformational deformation $\vec{y} = \mathbf{G}_i \cdot \vec{x}$ by a shear direction $\hat{m}_i$ and magnitude η_i, which in general will not be geometrically compatible from one hexagon to the next. The sheared hexagons can then be deformed elastically to enforce compatibility and folding of the sheet into a closed shell by the CK construction. If positions of material points on the final closed shell are denoted by mapping $\vec{z}(s^\alpha)$, then the elastic deformation is described by the mapping of differential elements $d\vec{y}$ in the sheared hexagons to elements $d\vec{z}$ of the tangent space of the shell surface, written as $d\vec{z} = \mathbf{F} \cdot d\vec{y}$. Pulling these differentials back to the symmetric reference configuration, we can write

$$\nabla\vec{z} \cdot d\vec{x} = d\vec{z} = \mathbf{F} \cdot d\vec{y} = \mathbf{F} \cdot \mathbf{G} \cdot d\vec{x} \quad \Rightarrow \quad \mathbf{F} = (\nabla\vec{z}) \cdot \mathbf{G}^{-1} = (\partial_\alpha \vec{z} \otimes \hat{a}^\alpha) \cdot \mathbf{G}^{-1},$$

where $\hat{a}^\alpha$ are the dual basis vectors such that $\hat{a}^\alpha \cdot \hat{a}_\beta = \delta^\alpha_\beta$. Differential lengths then transform as

$$d\ell'^2 = |d\vec{z}|^2 = d\vec{y} \cdot \mathbf{C} d\vec{y},$$

where $\mathbf{C} = \mathbf{F}^T \cdot \mathbf{F}$ is the metric tensor (commonly referred to as the right Cauchy-Green Deformation tensor) of the elastic deformation from $\vec{y}$ to $\vec{z}$. The nonlinear (Green-Lagrange) strain tensor $\mathbf{E} = \frac{1}{2}(\mathbf{C} - \mathbf{I})$ gives the relative change in lengths as

$$\frac{d\ell' - d\ell}{d\ell} \approx \frac{d\ell'^2 - d\ell^2}{2d\ell^2} \equiv \frac{d\vec{y}}{d\ell} \cdot \mathbf{E} \cdot \frac{d\vec{y}}{d\ell}.$$

The contribution of elasticity to the Landau free energy can be defined by a strain-energy density function parameterized either by the metric $w(\mathbf{C})$, or by the strain $w(\mathbf{E})$. For protein hexamers this function ought to obey the symmetries of the so-called "hexagonal-pyramidal" group [62, 63], defined by rotations $\theta \in \{-2\pi/3, +2\pi/3, \pi\}$ about the normal to the reference plane. To quadratic order the tensor invariants of this group are the isotropic invariants $I_1 = \mathrm{tr}\,\mathbf{C}$, and $I_2 = \frac{1}{2}[(\mathrm{tr}\,\mathbf{C})^2 - \mathrm{tr}\,(\mathbf{C}^2)]$. The elastic energy can then be truncated only to depend only on I_1 and I_2. For further simplification, we can separate the contributions of area dilatation $\sqrt{I_2} = J \equiv \frac{dA'}{dA}$, from area-preserving deformations parameterized by I_1/J. To lowest order this would give

$$w = \frac{K}{2}(J-1)^2 + \frac{\mu}{2}(I_1/J - 2) = \frac{K}{2}(\lambda_1\lambda_2 - 1)^2 + \frac{\mu}{2}\left(\frac{\lambda_1}{\lambda_2} + \frac{\lambda_2}{\lambda_1} - 2\right),$$

where λ_α are the square roots of the eigenvalues of $\mathbf{C}$ (the principal stretches).

The free energy of in-plane deformations, both elastic and conformational, can then be modeled with some generality as

$$\mathscr{F} = \int w(\mathbf{C}) dA + \sum_{i=1}^{10(T-1)} g(\eta_i).$$

The Landau energy g defines the free energy of the individual hexamers *in isolation*, which in general will depend on the detailed molecular interactions. Viewing conformational change as a chemical reaction, the conformational strain magnitudes η_i play the

role of *reaction coordinates* for the isolated hexamers. Through the definition of $g(\eta)$ we can model the kinetics of maturation. Because the deformation metric $\mathbf{C}$ measures the elastic strains, it depends both the displacement degrees of freedom $\vec{z}(s^\alpha)$ and on the conformational degrees of freedom $\eta(s^\alpha)$.

We should mention that similar generalizations of large-displacement elasticity theory have been applied to *growing tissue*, where one also is confronted with the problem of elastic stress in systems whose internal stress-free reference state should be treated as evolving in time (see for example, [64]). While it is often referred to as "morphoelasticity", one might be tempted to call this new area the "elasticity of life".

4.5 A View Askew

Applying this theory to the concrete example of HK97, we start from the observation that the initial hexamer skewing in the prohead state is driven by interactions among the so called Delta domains that line the interior surface of the capsid and that tense the hexamers. After these domains are cleaved, energy is released and the hexamers "spring" from the skewed to the symmetric configuration. This can be understood as a change in the Landau energy $g(\eta)$ from having a minimum at finite η (skew) to one at zero η (symmetric). A simple way to model the skewed prohead state is to fix η at a nonzero value, and relax the elastic strain energy of the shell [65]. This yields states of elastic strain and residual stress in the shell that are discontinuous across the interfaces between hexamers. The results are shown in Fig. 11 . Recall that in classical thin-shell elasticity theory there is a critical value γ_B for the dimensionless FvK Number YR^2/κ tat which the shell undergoes a buckling transition. Figure 11 gives, for fixed η, the critical FvK number $\gamma_B(\eta)$ for which the shell undergoes a buckling according the theory presented above. This critical FvK Number diverges around $\eta \simeq 0.2$. For the EI capsid, where

$\eta = 0$, the best fitted value is about ten times the buckling threshold. Our theory predicts that, if we increase η, a reverse buckling transition takes around $\eta \simeq 0.15$. The η value of the Prohead structure, which is about 0.2, is larger so the Prohead structure should be roughly spherical, as indeed is the case. In the Prohead structure, the residual stresses of the conformational strains counteract the stress-field due to the pentamer disclinations, resulting in shells that are close to spherical in shape.

The next step is to minimize the full free energy with respect to η. The scission of the Delta domains is described in Landau theory as an exchange of the absolute minimum of $g(\eta)$ from $\eta \simeq 0.2$ to $\eta \simeq 0$. This, in turn, drives a buckling transition as described above. Landau theory has provided us with a connection between events at the molecular level, as described by the change of $g(\eta)$, to events at the level of the shape of the capsid as a whole. For η greater than 0.2, the capsid adopts a dodecahedral shape (see Fig. 11). In this regime, it would no longer be possible to fit the capsid shape with the LMN thin-shell elasticity theory that uses CK icosahedra as the reference state, though it might be possible to do so with a thin-shell elasticity theory that starts from a perfect dodecahedron as the reference state. The advantage of the generalized theory over thin-shell elasticity theory is thus that it has removed the dependency on the choice of the stress-free reference state.

As we step back to look at the overall structure of the Landau theory of capsid maturation, it becomes clear that it offers a more generic framework for macromolecular assemblies in general. The Caspar-Klug idea of quasi-equivalence must be generalized to the notion that the conformation of a protein subunit as it interacts with others in a large assembly may be very different from its conformation in isolation. When defining a theory of macromolecular elasticity, what conformation should be taken as the stress-free reference configuration? It may indeed be neither the assembled nor isolated

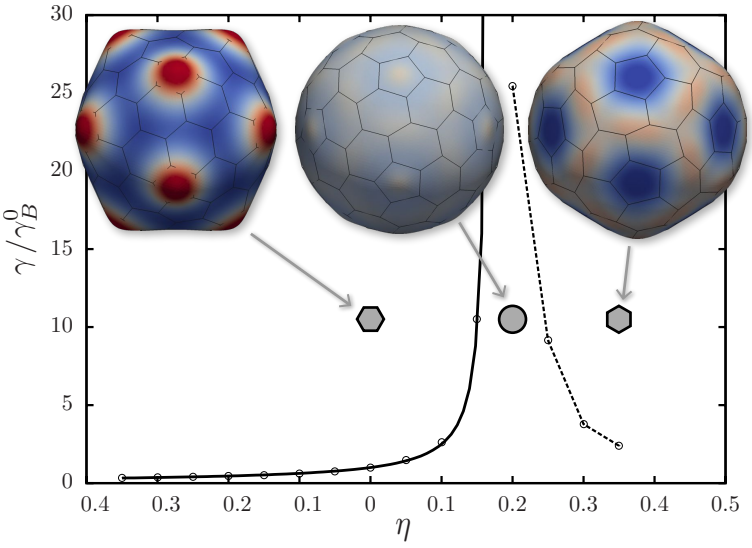

Figure 11: Phase diagram of the HK97 Prohead-to-Expansion-Intermediate transition as a structural phase change. The critical FvK number γ_B (solid and dashed lines) is defined as the value of γ at which the shell is buckled.

conformations. Most generally, the reference configuration of the units in an assembly should be treated theoretically as an *internal variable*. Together, Landau theory and nonlinear, finite-deformation continuum elasticity provide a general framework for theoretical treatment of the mechanics of macromolecular aggregates including both elastic and conformational degrees of freedom. In principle, the framework also outlines a systematic path toward multiscale modeling of such systems: detailed molecular models can be used to identify key conformational modes, and parameterize the energetics of "internal" conformational degrees of freedom, which can then be inserted into the continuum theory in the form of a Landau energy to understand coupling to elasticity on larger length scales.

4.6 An Armour for a Molecular Machine

The maturation of HK97 is an amazing sequence of transformations. But what is the point of this molecular dance? We mentioned that viruses with double-stranded DNA genomes are able to withstand very large internal pressures. The sequence of displacements of the HK97 shell is coupled to a parallel sequence of coordinated chemical reactions taking place across the outer surface of the capsid. The CP of HK97 has two relatively flexible loops, called the E and P loops. One specific residue on the E loop (a lysine residue) is capable of forming a covalent chemical bond with another specific residue on the P (an arginine residue). It is not possible for the E and P loops of the same CP to be stapled together – as they are to far away from each other – but adjacent CPs can form such a bond [50]. In the initial, highly strained EI-I/II states, the P loop is rotated away and it is not possible to establish such bonds. As the shell passes through its sequence of transformation the CPs are knitted together by a progressively more complex pattern of covalent bonds, as shown in Fig. 12. In the end, the capsid covered by a mesh of interlocking rings resembling chain mail. The structural transformations provide a changing stage for the orderly formation of these chemical bonds so the final capsid can withstand the large pressures exerted by the genome. We speculate that the soft modes of the shell may play an important role in the establishment of the bonds: thermally excited soft modes may allow the E and P loops of adjacent CPs to search each other in preparation of establishing a chemical bond, which could be viewed as a molecular dating service.

We have moved very far indeed from the notion that viral capsid are just containers characterized by a T-Number. The capsid of HK97 is truly an active molecular machine that transforms elastic and chemical energy into the synthesis of a shell that is one gigantic spherical molecule. The basic fold of HK97 that enables this extraordinary form

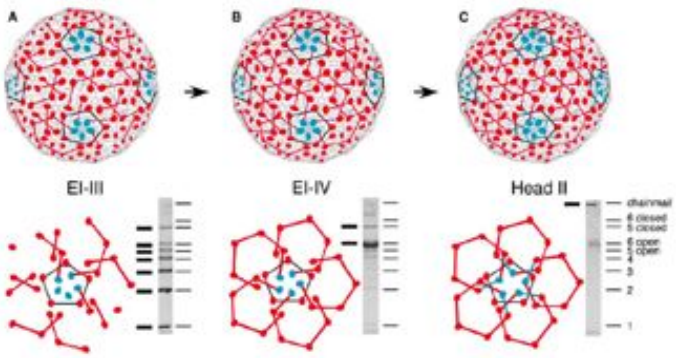

Figure 12: Spreading of covalent bonds over the HK97 capsid during maturation. From Ref.[66]. The CPs are represented as ovals, hexamers are in red and pentamers in blue. During the first step (A), pentamers are lined by closed rings of bonds. In the second step (B), hexamers are linked by open rings. In the final steps (C), the rings close forming an interlocking mesh.

of physico-chemical wizardry is encountered in many other viruses, including the Herpes virus. One can at least hope that materials science will be able to develop synthetic versions of these devices but we fully expect that the exploration of the working of viral molecular machines will provide new opportunities for the application of methods borrowed from statistical physics, elasticity theory, and condensed-matter physics.

Acknowledgements

We wish to thank Joseph Rudnick, our long-time collaborator, for many productive discussions and interactions. We benefited from our collaborations with A. Aggarwal, T. Guerin, A. Morozov, T. Nguyen, L. Perotti, T. Luque Santolaria, R. Zandi and discussions in the UCLA virus group led by W. Gelbart and C. Knobler. We would like to thank C. Knobler for correcting the first draft of the manuscript. We would like to thank our colleagues M. Hagan, P. van der Schoot, and A. Zlotnick for helpful discussions. We

thank the NSF for support under grants CMMI-0748034, DMR-1006128, and DMR-1309423.

References

1. Fraenkel-Conrat H, Williams R, Proc. Nat. Acad. Sci. USA 41:690 (1955).
2. Mao C, et al., Science 303:213 (2004).
3. Bancroft J, Hills G, Markham R, Virology 32:354 (1967).
4. Speir J, Munshi S, Wang G, Baker T, Johnson J, Structure 3:63 (1995).
5. Baker S, Olson N, Microbiol. and Mol. Biol. Rev 63:862 (1999).
6. Adolph K, Butler P, J. Mol. Biol. 88:327 (1974).
7. Safran S, *Statistical thermodynamics of surfaces, interfaces, and membranes* (Addison-Wesley Reading, MA, 1994).
8. Brandon C, Toze J, *Introduction to Protein Structure* (World Scientific Publishing Company, 1999).
9. Kegel W, van der Schoot P, Biophys. J. 91:1501 (2006).
10. Kegel W, van der Schoot P, Biophys. J. 86:3905 (2004).
11. Rapaport D, Physi. Rev. Lett. 101:186101 (2008).
12. Elrad O, Hagan M, Physical Biology 7:045003 (2010).
13. Nguyen H, Reddy V, Brooks C, J Am Chem Soc. 131:2606 (2009).
14.
15. Caspar D, Klug A, Cold Spring Harbor Symp. Quant. Biol. 27:1 (1962).
16. Hendrix R, Adv.Virus Res. 64:1 (2005).

17. Bruinsma R, Gelbart W, Reguera D, Rudnick J, Zandi R, Phys. Rev. Lett. 90:248101 (2003).

18. Johnson J, Tang J, Nyame Y, Willits D, Young M, Zlotnick A, Nano Lett. 5:765 (2005).

19. Berger B, Shor P, Tucker-Kellogg L, King J, Proc Natl Acad Sci U S A 91:7732 (1994).

20. Tarnai T, Gaspar Z, Acta Crystallographica A 43:612 (1987).

21. Zandi R, Reguera D, Bruinsma RF, Gelbart WM, Rudnick J, Proceedings of the National Academy of Sciences of the United States of America 101:15556 (2004).

22. Zlotnick A, J. Mol. Biol. 366:14 (2007).

23. Zlotnick A, J. Mol. Biol. 241:59 (1994).

24. Morozov A, Bruinsma R, Rudnick J, J. Chem. Phys. 131:155101 (2009).

25. van Kampen N, *Stochastic Processes in Physics and Chemistry* (Elsevier, 2007).

26. Hagan M, Elrad O, Biophys. J. 98:1065 (2010).

27. Casini G, Graham D, Heine D, Garcea R, Wu D, Virology. 325:320 (2004.).

28. Zlotnick A, Aldrich R, Johnson J, Ceres P, Young M, Virology 277:450 (2000).

29. Endres D, Zlotnick A, Biophys J.. 83:1217 (2002.).

30. Hagan M, Chandler D, Biophys. J. 91:42 (2006).

31. Morozov A, Rudnick J, Bruinsma R, Klug W, *Emerging Topics in Physical Virology edited by P.Stockley and R.Twarock* (World Scientific Publishing Company, 2010).

32. Luque A, Reguera D, Morozov A, Rudnick J, Bruinsma R, J.Chem.Phys. 136:184507 (2012).

33. Langer J, Rev. Mod. Phys 52:1066 (1980).

34. Morozov A, Bruinsma R, Phys.Rev.E 81:041925 (2010).

35. Joseph D, Elser V, Phys. Rev. Lett. 79:1066 (1997).

36. Zink M, Grubmüller H, Biophys. J. 96:1350 (2009).

37. Shepherd CM, Borelli IA, Lander G, Natarajan P, Siddavanahalli V, et al., Nucleic acids research 34:D386 (2006).

38. Kinjo AR, Suzuki H, Yamashita R, Ikegawa Y, Kudou T, et al., Nucleic acids research 40:D453 (2012).

39. Pettersen EF, Goddard TD, Huang CC, Couch GS, Greenblatt DM, et al., Journal of computational chemistry 25:1605 (2004).

40. Lidmar J, Mirny L, Nelson DR, Physical Review E 68:051910 (2003).

41. Roos W, Bruinsma R, Wuite G, Nature Physics. 6:733 (2010.).

42. Seung H, Nelson DR, Physical Review A 38:1005 (1988).

43. Widom M, Lidmar J, Nelson DR, Phys. Rev. E 76:031911 (2007).

44. Tama F, Brooks CL, J. Mol. Biol. 345:299 (2005).

45. Nguyen T, Bruinsma RF, Gelbart WM, Physical Review E 72:051923 (2005).

46. Levandovsky A, Zandi R, Physical review letters 102:198102 (2009).

47. Klug WS, Bruinsma RF, Michel JP, Knobler CM, Ivanovska IL, et al., Phys.Rev.Lett. 97:228101 (2006).

48. Johnson JE, Curr. Opin. Struct. Biol. 20:210 (2010).

49. Conway J, Wikoff W, Cheng N, Duda R, Hendrix R, et al., Science 292:744 (2001).

50. Lee KK, Gan L, Tsuruta H, Moyer C, Conway JF, et al., Structure 16:1491 (2008).

51. Gertsman I, Gan L, Guttman M, Lee K, Speir JA, et al., Nature 458:646 (2009).

52. Conway JF, Duda RL, Cheng N, Hendrix RW, Steven AC, J. Mol. Biol. 253:86 (1995).

53. Jiang W, Li Z, Zhang Z, Baker ML, Prevelige PE, Chiu W, Nature Structural & Molecular Biology 10:131 (2003).

54. Dokland T, Murialdo H, Journal of molecular biology 233:682 (1993).

55. Lander GC, Baudoux AC, Azam F, Potter CS, Carragher B, Johnson JE, Structure 20:498 (2012).

56. Preux O, Durand D, Huet A, Conway JF, Bertin A, et al., Journal of molecular biology 425:1999 (2013).

57. Cheng N, Trus BL, Belnap DM, Newcomb WW, Brown JC, Steven AC, Journal of virology 76:7855 (2002).

58. Khachaturyan A, *Theory of Structural Transformations in Solids* (Dover Publications, 1983).

59. Guerin T, Bruinsma R, Phys Rev E22049-54. 76:061911 (2007.).

60. Tama F, Brooks III CL, J. Mol. Biol. 318:733 (2002).

61. Tama F, Brooks III CL, Annu. Rev. Biophys. Biomol. Struct. 35:115 (2006).

62. Smith G, Rivlin R, Trans. Amer. Math. Soc 88:1976 (1958).

63. Green A, Adkins J, *Large Elastic Deformations* (Clarendon Press (Oxford), 1970).

64. Liang H, Mahadevan L, Proc Natl Acad Sci U S A. 106:22049 (2009.).

65. Aggarwal A, Rudnick J, Bruinsma R, Klug W, Phys.Rev.Lett. 109:148102 (2012).

66. Gan L, Conway J, Firek B, Cheng N, Hendrix R, et al., Molecular Cell. 114:559 (2004).